Mechanistic insights into the role of polydopamine interlayer towards improved separation performance of polyamide nanofiltration membranes

Zhe Yang,[a] Fei Wang,[a] Hao Guo,[a] Lu Elfa Peng,[a] Xiao-hua Ma,[b] Xiao-xiao Song,[c*]

Zhiwei Wang,[d] and Chuyang Y. Tang[a*]

[a] Department of Civil Engineering, the University of Hong Kong, Pokfulam, Hong Kong, SAR, P. R. China

[b] School of Chemical Engineering, East China University of Science and Technology, Meilong Road 130, Shanghai 200237, P. R. China

[c] Center for Membrane and Water Science & Technology, Ocean College, Zhejiang University of Technology, Hangzhou, 310014, P. R. China

[d] State Key Laboratory of Pollution Control and Resource Reuse, Shanghai Institute of Pollution Control and Ecological Security, School of Environmental Science and Engineering, Tongji University, Shanghai 200092, China

[*] Corresponding Author.

Phone: +852 2859 1976, Fax: +852 2559 5337, E-mail address: tangc@hku.hk

Phone: +86 (0571) 8832 4135; Email: songxiaoxiao@zjut.edu.cn

ABSTRACT

Interlayered thin-film nanocomposite membranes (TFNi) are an emerging type of membranes with great potential to overcome the permeability-selectivity upper bound of conventional thin-film composite (TFC) nanofiltration and reverse osmosis membranes. However, the exact roles of the interlayer and the corresponding mechanisms leading to enhanced separation performance of TFNi membranes remain poorly understood. This study reports a polydopamine (PDA) intercalated TFNi nanofiltration membrane (PA-PSF2, PDA coating time at 2hr) that possessed nearly an order of magnitude higher water permeance of 14.8 ± 0.4 $Lm^{-2}h^{-1}bar^{-1}$ compared to the control TFC membrane (PA-PFS0) of 2.4 ± 0.5 $Lm^{-2}h^{-1}bar^{-1}$. The TFNi membrane further showed enhanced rejection towards a wide range of inorganic salts and small organic molecules (including antibiotics and endocrine disruptors). Detailed mechanistic investigation reveals that the membrane separation performance was enhanced due to both the direct “gutter” effect of the PDA interlayer and its indirect effects resulting from enhanced polyamide formation on the PDA-coated substrate, with the “gutter” effect playing a more dominant role. This study provides a mechanistic and comprehensive framework for the future development of TFNi membranes.

TOC art

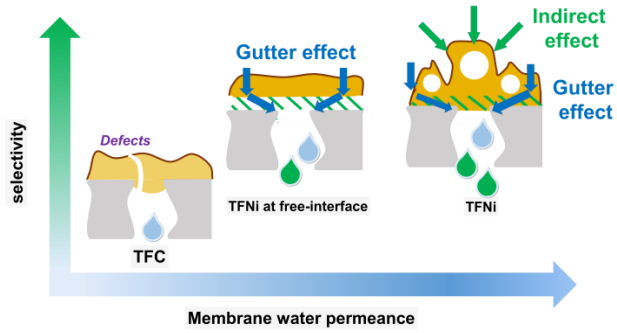
selectivity
Defects
TFC
Gutter effect
TFNi at free-interface
Indirect effect
Gutter effect
TFNi
Membrane water permeance

INTRODUCTION

Thin-film composite (TFC) reverse osmosis (RO) and nanofiltration (NF) membranes, consisting of an ultra-thin (~100 nm) polyamide selective layer on an ultrafiltration substrate, are the core for membrane-based desalination and water reuse.[1, 2] However, conventional TFC membranes are strongly constrained by the "upper bound" trade-off between their water permeance and selectivity.[3] Recently, a new class of thin-film nanocomposite membranes with an interlayer structure (TFNi) have been reported.[4-6] Up to date, a wide range of interfacial coatings have been applied (e.g., polyelectrolytes,[5] polydopamine (PDA),[7-11] polyphenols,[12] poly(ether ether ketone),[13] halloysite nanotubes,[14] carbon nanotubes,[6, 15-17] and their derivatives,[18, 19]), with some studies showing an order of magnitude higher water permeance and simultaneously enhanced water/solute selectivity for TFNi membranes.[15, 19, 20]

Despite the great potential of TFNi membranes to overcome the longstanding permeability-selectivity upper bound,[3] experimental results often show contradictory trends. For example, PDA has been one of the most commonly applied coating materials due to its simplicity, strong adhesion, hydrophilicity, and ease for thickness control.[21, 22] Many studies have reported PDA as an interlayer coating for the preparation of TFNi membranes.[7, 8, 23, 24] While some studies observed enhanced membrane permeance for PDA intercalated membranes,[8, 10, 18] others reported a slight reduction in permeance.[7, 24] Systematic studies are needed to better resolve the

fundamental mechanisms governing the role of interlayers. In addition, the existing literature on TFNi membranes focuses primarily on salt removal efficiency in the context of desalination.[7, 10, 23, 25] On the other hand, the removal of trace organic contaminants (TrOCs) can be far more important than the removal of simple salts for some important applications such as potable water reuse.[2, 26] These literature gaps prompt us to perform a systematic mechanistic investigation on the fundamental roles of interlayers in membrane formation and in the transport of water, salts, and organic micropollutants through TFNi membranes.

In this study, we use PDA as a model interlayer to investigate its impact on the formation of polyamide NF membranes and their separation performance. We hypothesize that the enhanced water permeance of TFNi membranes is contributed by the combined effects of (1) the shortened transport pathway through the rejection layer upon the inclusion of a highly permeable interlayer (similar to the gutter effect in the context of gas separation[27]) and (2) the improved formation of the rejection layer itself. Polyamide rejection layers were formed on PDA-coated substrates by interfacial polymerization (IP) of piperazine (PIP) and trimesoyl chloride (TMC). We reveal the critical roles of the PDA interlayer on the gutter effect and on the physiochemical properties of the polyamide layers, thereby elucidating the governing mechanisms responsible for enhanced water permeance, salt rejection, and TrOCs removal of the TFNi membranes. For the first time, the relative contributions of the

85 direct gutter effect and indirect effect through enhanced membrane formation are
86 resolved. This study provides critical mechanistic insights to the design and
87 fabrication of next-generation high-performance NF membranes.
88

MATERIALS AND METHODS

Materials and chemicals.

Unless described otherwise, all solutions were prepared from analytical-grade chemicals and Millipore ultrapure water. Polysulfone (PSF, Mw. 35,000), N, N-dimethylformamide (DMF, anhydrous 99.8%), piperazine (PIP, ReagentPlus®, 99%), trimesoyl chloride (TMC, 98%), and hexane (HPLC grade, 95%) were all purchased from Sigma-Aldrich for the fabrication of PSF substrates and TFC NF membranes. Sodium chloride (NaCl), sodium sulfate anhydrous (Na_2SO_4), magnesium chloride ($MgCl_2$ 6-hydrate), magnesium sulfate ($MgSO_4$) and calcium chloride anhydrous ($CaCl_2$) were all purchased from Uni-Chem chemical reagents. D-(+)Glucose (Mw. 180.16, Diekmann), D-Raffinose (Mw 504.44, Macklin) and Dextran (Mw 1000 and 2000, D-chem) were used for the evaluation of the pores size of the fabricated TFC membranes. Dopamine hydrochloride (J&K Scientific Ltd., China), tris (hydroxymethyl, Acros Organics, Geel, Belgium) and hydrochloric acid (HCl, 37 wt%, VWR, Dorset, U.K) were obtained for preparing PDA coating. Chloroform (VWR, Dorset, U.K) was used as a solvent for isolating polyamide rejection layers. Two endocrine-disrupting compounds (ethylparaben (MW = 166.2 Da) and propylparaben (180.2 Da)) and four antibiotics (sulfamethoxazole (253.3 Da), sulfamethazine (278.3 Da), norfloxacin (319.3 Da), and ofloxacin (361.4 Da)) were used as model TrOCs, and all these compounds were purchased from Sigma-Aldrich.

Synthesis of TFNi membranes.

A PSF substrate was first fabricated by the phase inversion method using a polymer dope of 15 wt% PSF dissolved in DMF following our previous study.[19] PDA coating was performed by pouring a 2 g/L dopamine solution containing 10 mM Tris-HCl buffer at pH 8.5 to a membrane coupon placed in a home-made container in such a way that only its front side was exposed to the coating solution over predetermined time duration (1, 2 or 24 hr) under continuous shaking. The PDA-coated PSF substrate was denoted as PSFn, where n represents the PDA coating duration (with n = 0 indicating no PDA coating).

To synthesize the TFNi membrane, an IP reaction was performed on the pristine or PDA-modified PSF (Figure 1). Briefly, a 0.2 wt% PIP/H_2O solution was gently poured onto the substrate for 3 min. The excess solution was removed by a rubber roller. Then, a 0.15 wt% TMC/hexane solution was introduced to the PIP-impregnated substrate, and the IP reaction was continued for 1 min. Subsequently, the fabricated membrane was rinsed by hexane to remove the unreacted TMC and was further post-treated in an oven for 10 min at 60 ºC. The resultant TFNi membrane, denoted as PA-PSFn in accordance to its substrate, was stored in deionized water before further use. In this study, PA-PSF0 stands for the control TFC membrane prepared on the pristine PSF substrate without PDA coating.

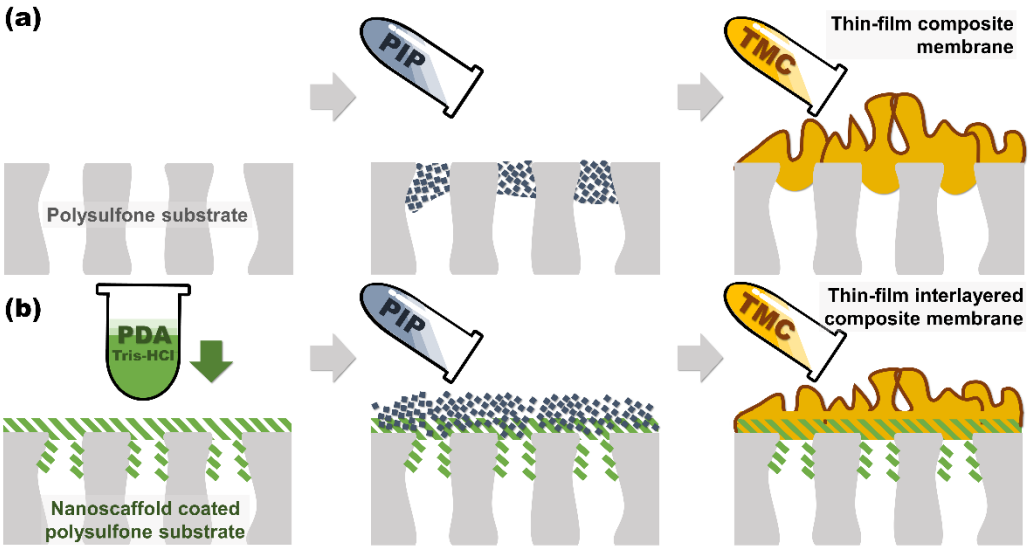

Figure 1. Schematic diagram on the fabrication of TFC (a) and TFNi membranes (b). To prepare the PDA interlayer, a dopamine solution (2g/L in 10 mM Tris-HCl buffer at pH 8.5) was used to coat the substrate for a predetermined duration (1, 2 or 24 hr). Interfacial polymerization was performed on the substrates with or without PDA coating to obtain TFNi and TFC membranes, respectively. The concentration of PIP was 0.2 wt% and that of TMC was 0.15 wt%.

Synthesis of polyamide nanofilms at free aqueous-organic interface.

In order to resolve the role of the interlayer on membrane transport properties (e.g., its direct effect as a high-permeability gutter layer[27] vs. its indirect effect on the formation of the polyamide layer[19, 28]), we further synthesized polyamide nanofilms at a free interface (PAfi) between an aqueous solution (0.2 wt% PIP/H_2O) and an organic solution (0.15 wt% TMC/hexane).[29] Formation of polyamide nanofilms at free interfaces has been well documented in the literature.[5, 25, 29] The properties of the generated polyamide nanofilms depend only on the composition monomer solutions and the reaction time, while the interference of the substrate is prevented. In the current study, the use of identical IP reaction conditions (monomer solutions and

148 reaction time) led to identical polyamide nanofilms. The nanofilms were
149 vacuum-filtrated (filtration time = 1 min) onto the pristine PSF0 substrate and a
150 PDA-coated PSF2 substrate, and the resulting membranes PAfi-PSF0 and PAfi-PSF2
151 were then washed by hexane and heat-treated for 10 min at 60°C. In the current study,
152 PAfi-PSF0 and PAfi-PSF2 have identical rejection layers. Therefore, the difference
153 between their transport properties is attributed to the direct effect of interlayer on the
154 substrate. In contrast, the difference between PA-PSF0 and PA-PSF2 can be caused by
155 both the direct effect of the substrate and additional indirect effects, noting that the
156 morphology and chemistry of the polyamide layers could be potentially affected by
157 the presence of the interlayer.
158
159 **Membrane characterization.**
160 Surface morphology of the membranes and substrates was examined by scanning
161 electron microscope (SEM, LEO 1530, FEG UK) using an accelerating voltage of 5
162 kV. Prior to the characterization, the membranes samples were coated by platinum and
163 gold for 40 seconds. In addition to the front surfaces, the back surfaces of the
164 rejection layers of PA-PSFn membranes were also examined by SEM after dissolving
165 PSF using chloroform following our previous study.[19] Specifically, a piece of
166 membrane specimen (0.5 cm × 0.5 cm) was attached onto a silicon wafer, with its
167 polyamide side facing the silicon wafer. Chloroform, a solvent frequently reported in
168 the literature[19, 30] for dissolving PSF to isolate the polyamide layer, was applied to

rinse the PSF substrate until the white precipitations completely dissappeared from the sample. According to our previous study,[19] this procedure ensures the complete removal of the PSF substrate.

Membrane cross-sectional images were obtained using a transmission electron microscope (TEM, Philips CM100, Eindhoven, Netherlands) at an accelerating voltage of 100 kV.[31] The thickness of the rejection layer was determined from TEM micrographs using image software (MediaCybernetics, Inc.). Membrane roughness of the front and back surface of the rejection layers was measured by atomic force microscopy (AFM, Multimode 8, Bruker, MA) with a scanning size of 5 × 5 μm. The value of root-mean-square roughness (Rq) and maximum roughness (Rmax) was obtained using the Nanoscope Analysis software (Bruker, MA). Membrane water contact angle was measured using an automatic contact angle meter (Attension Theta, Biolin Scientific, Sweden) equipped with a video capture device. A membrane specimen was vacuum-dried at room temperature for 24 hr before the measurement. A water droplet of approximately 3 μL was placed on the membrane surface and the contact angle was recorded after a stabilizing time of 10 s. For each membrane type, the contact angle measurements were repeated at 10 different locations for two different membrane samples, and the average value was reported. Membrane functional groups and surface elemental compositions were characterized using attenuated total reflection Fourier transform infrared (ATR-FTIR) spectroscopy and

X-ray photoelectron spectroscopy (XPS), respectively.[31-33] A quartz crystal microbalance with dissipation (QCM-D, E4, Q-Sense Biolin Scientific, Sweden) was used to quantify the amount of PIP uptake by the control PSF0 and PDA-coated PSFn substrates following our previous study.[19]

Separation performance testing.

Membrane separation performance was tested using a cross-flow filtration setup at 24 °C. A membrane coupon (20.6 cm^2) was subjected to an applied pressure of 50 psi (i.e., 3.45 bar) for 1 hr before the measurement of water flux and salt rejection under the same pressure. Additional tests were also included to study the effect of applied pressure on membrane separation performance (see Supporting Information S3). Water flux was determined by weighing the mass of the permeate over a designated time interval:

$$J_v = \frac{\Delta m}{\Delta t \times A \times \rho} \quad (1)$$

where J_v (L m^{-2} h^{-1}) is the water flux, Δm (kg) is the mass of the permeate collected over a duration of Δt (h), A (m^2) is the effective membrane area, and ρ (kg L^{-1}) is the density of the permeate water. The membrane water permeance was determined as the ratio of pure water flux over the applied pressure.

The salt rejection was measured using a feed solution containing a single type of salt (1000 ppm Na_2SO_4, $MgSO_4$, $MgCl_2$, $CaCl_2$, or NaCl). For each test, a new membrane

coupon was pre-compacted for 1 hr before the collection of permeate samples. The salt rejection R was determined based on the conductivity of the feed (C_f) and that of the permeate (C_p) measured by a conductivity meter (Ultrameter II, Myron L company, Carlsbad, CA) using Equation (2). The reported rejection is the average value of three membrane samples from different batches. The separation factor (α) of NaCl to $MgSO_4$ was calculated based on Equation (3).

$$R = (1 - \frac{C_p}{C_f}) \times 100\% \quad (2)$$

$$\alpha = \frac{(C_{NaCl} / C_{MgSO_4})_p}{(C_{NaCl} / C_{MgSO_4})_f} = \frac{1 - R_{NaCl}}{1 - R_{MgSO_4}} \quad (3)$$

The rejection of TrOCs (ethylparaben, propylparaben, sulfamethoxazole, sulfamethazine, norfloxacin and ofloxacin) were also evaluated based on our previous work.[34, 35] Briefly, a feed solution containing a cocktail of TrOCs (200 μg/L for each compound) was prepared by introducing 1 mL stock solution of each TrOC (1g/L in methanol) to the feed tank (5 L). An equilibrium time of 12 h was allowed, before feed and permeate samples were collected for further analysis using an ultraperformance liquid chromatograph with double mass spectra (UPLC-MS/MS, Waters ACQUITY).[36] According to the literature, the equilibrium time ensures stable rejection performance (e.g., by eliminating the potential effect of TrOC sorption by the membrane).[36-38] The rejection of each TrOC was determined based on the measured feed (C_f) and permeate (C_p) concentrations (Equation (2)) using three

different membrane samples.

RESULTS AND DISCUSSIONS

Properties of PSFn substrates.

Figure 2 presents the properties of the substrates. Compared to the pristine PSF0, the PDA-coated substrates became increasingly darker at longer coating time, which is in good agreement with the literature.[22, 39] The contact angle decreased from 92.6 ± 5.3° for PSF0 to 35.3 ± 2.6° for PSF24, which can be attributed to the hydrophilic amine and catechol groups of PDA.[21, 40] The water permeance of the substrate decreased mildly after short-duration coating (274.5 ± 35.9 and 242.3 ± 46.8 $Lm^{-2}h^{-1}bar^{-1}$ for PSF1 and PSF2, respectively, compared to 314.8 ± 14.6 $Lm^{-2}h^{-1}bar^{-1}$ for PSF0). This trend is consistent with the decreased substrate pore size after PDA coating (Figure 3a). This decrease in pore size was likely due to the penetration of PDA into substrate pores.[8, 23] At a coating duration of 24 hr, a large number of PDA aggregates appeared (Figure 3a) – a phenomenon also reported in prior studies.[7] Although the PSF24 substrate with the extended coating duration had the lowest water contact angle, its surface pores were extensively covered by PDA, resulting in a dramatically reduced water permeance of 41.3 ± 9.0 $Lm^{-2}h^{-1}bar^{-1}$ for PSF24.

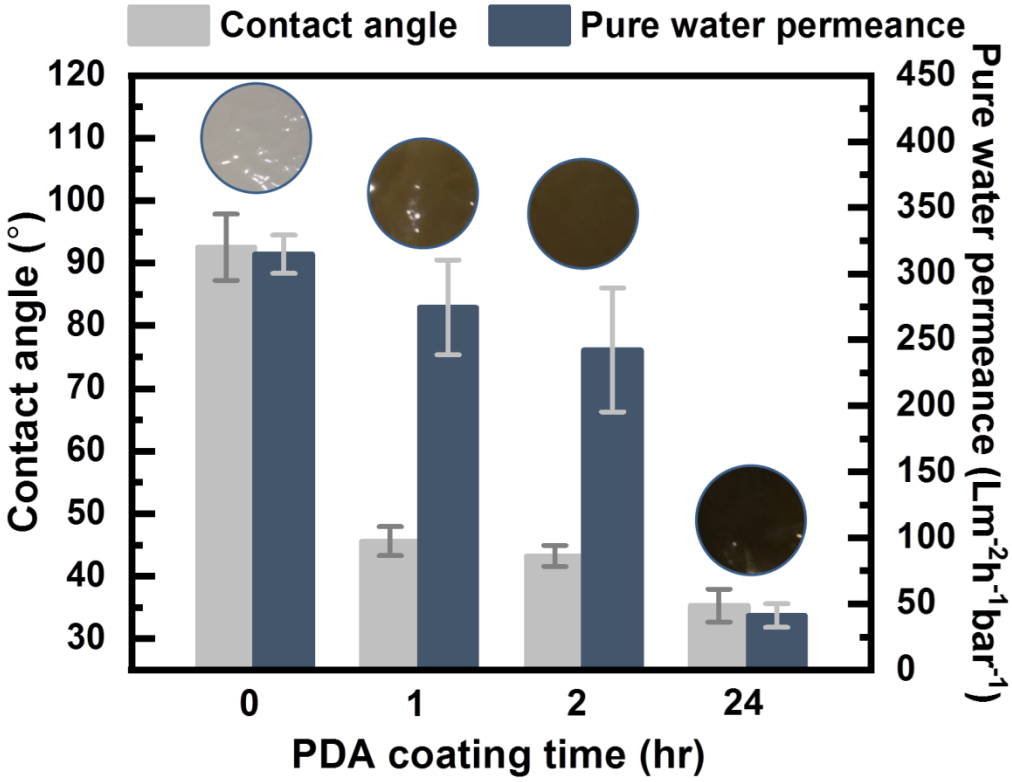

Figure. 2. Contact angle and water permeance of the substrates. Digital photos of the substrates are also shown.

Properties of PA-PSFn membranes.

ATR-FTIR results (Supporting Information S1) confirm the formation of polyamide layers after the IP reaction.[41, 42] Figure 3b-e present the morphological features of the PA-PSFn membranes. Both SEM top views (Figure 3b) and TEM cross-sectional views (Figure 3d) show much rougher polyamide surfaces for PA-PSF2 and PA-PSF24, which is further confirmed by AFM results (Figure 3e and Table 1). In contrast, the bottom surface of the rejection layers was smoother for the TFNi membranes (PA-PSF1, PA-PSF2, and PA-PSF24) compared to the control PA-PSF0 (Figure 3c and Table 1). Indeed, the bottom surface of PA-PSF0 had numerous protuberances of several tens to hundreds of nm in size (Figure 3c), which was formed by the intrusion of polyamide into the large-sized pores of its substrate.[15, 19, 43] The much smoother bottom surfaces of the TFNi rejection layers revealed that PDA interlayers were able to prevent such undesirable intrusion of polyamide as a result of reduced pore size for coated substrates.[19]

The apparent thickness of the rejection layer of PA-PSF1 was comparable to that of the control membrane PA-PSF0 (60 - 70 nm, see TEM cross-sections in Figure 3c). In contrast, those of PA-PSF2 and PA-PSF24 were significantly thicker (116 ± 24 and 201 ± 37 nm, respectively), which agree well with their much greater surface roughness. Interestingly, the rejection layers of these two membranes contained discrete nanovoids that are not observed for PA-PSF0 and PA-PSF1 (magnified TEM

cross-sections images are available in Supporting Information S1). The presence of nanovoids has been frequently reported for fully aromatic polyamide prepared from m-phenylenediamine (MPD) and TMC.[30, 44, 45] Our prior studies suggest that CO_2 dissolved in the high-pH aqueous amine solution plays a critical role in forming such nanovoids: (1) the acid and heat produced during the IP reaction cause the interfacial degassing of CO_2 nanobubbles ($HCO_3^- + H^+ \xrightarrow{\Delta} CO_2\uparrow + H_2O$);[46, 47] (2) these nanobubbles are retained between the substrate and the polyamide layer, resulting in the formation of nanovoids accompanied with increased surface roughness.[46-48] Although such nanovoids are less frequently observed for semi-aromatic polyamide prepared from PIP and TMC due to the slower reaction and less reaction heat generated,[46] the current study show the feasibility to enhance nanovoid formation by introducing an interlayer. This enhanced nanovoid formation is likely due to the combined effects of (1) greater PIP sorption at longer PDA coating duration (Figure 4a) and thus greater interfacial heating effect;[29, 49] and (2) the improved gas confinement as a result of smaller surface pore size of the PDA-coated substrates.[28, 48] The presence of nanovoids in PA-PSF2 and PA-PSF24 partially explains their greater surface roughness, although that of PA-PSF24 could also be affected by the rough surface of its substrate (Figure 3a). According to the literature, these nanovoids are beneficial to provide thinner intrinsic polyamide thickness (i.e., the true thickness excluding nanovoids), increased effective filtration area, and enhanced water transport pathways.[44, 45, 50, 51] In current study, the contact angle (Table 1) was not significantly

affected by the PDA interlayer.

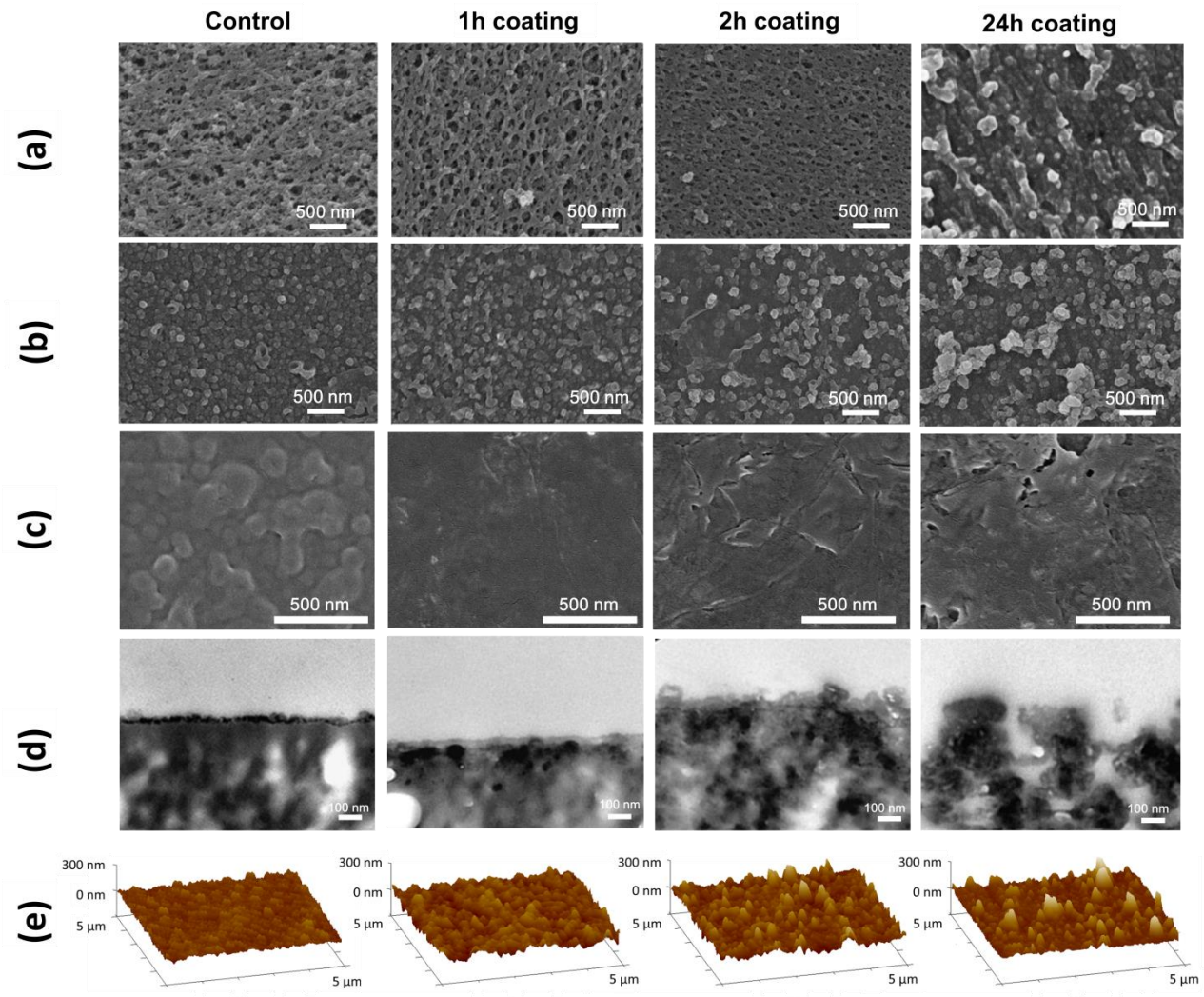

Figure 3. Microscopic characterization of PSFn substrates and PA-PSFn membranes: (a) SEM micrographs of substrate surfaces; (b) SEM micrographs of the top surfaces of PA-PSFn; (c) SEM micrographs of the bottom surfaces of the rejection layers isolated from PA-PSFn; (d) TEM micrographs of the cross-sections of PA-PSFn; and (e) AFM micrographs of the surface morphology of PA-PSFn. The scale bar for SEM is 500 nm and the scale bar for TEM is 100 nm.

306 Table 1. Roughness and water contact angle results of the PA-PSF membranes.

	Top surface of rejection layer		Bottom surface of rejection layer		Contact angle of membrane top surface
	*R*q (nm)	*R*max (nm)	*R*q (nm)	*R*max (nm)	(°)
PA-PSF0	18.4 ± 1.5	150.7 ± 10.4	44.2 ± 8.9	244.7 ± 19.1	53 ± 4
PA-PSF1	30.8 ± 2.4	221.0 ± 20.2	13.7 ± 2.6	111.1 ± 18.1	55 ± 4
PA-PSF2	36.2 ± 1.1	283.3 ± 14.7	18.3 ± 2.7	122.8 ± 12.8	54 ± 2
PA-PSF24	32.6 ± 0.8	318.7 ± 18.2	20.3 ± 1.4	134.3 ± 17.3	49 ± 2

307

308 Figure 4b presents the O:N ratio and crosslinking degree, both calculated from the
309 XPS results (Supporting Information S1). The O:N ratio of the PA-PSF1 (1.28 ± 0.03)
310 was significantly lower than that of the control PA-PSF0 membrane (1.50 ± 0.07),
311 revealing an enhanced crosslinking degree[34] with the introduction of the PDA
312 interlayer (63.3 ± 3.7% for PA-PSF1 vs. 41.0 ± 5.2% for PA-PSF0). At longer PDA
313 coating duration, the crosslinking degree was further improved. This result can be
314 well explained by the enhanced PIP sorption by the PDA-coated substrates (Figure
315 4a), with a greater effective PIP concentration in the IP reaction leading to a more
316 crosslinked polyamide.[7] Consistent with the XPS-based crosslinking analysis, pore
317 size analysis based on the rejection of neutral solutes (Figure 4c and Supporting
318 Information S2) shows that the TFNi membranes with PDA-coated substrates had
319 significantly smaller effective mean pore sizes (μ_p ~ 0.34-0.36 nm) compared to that
320 of the control PA-PSF0 membrane (μ_p ~ 0.51 nm).

321

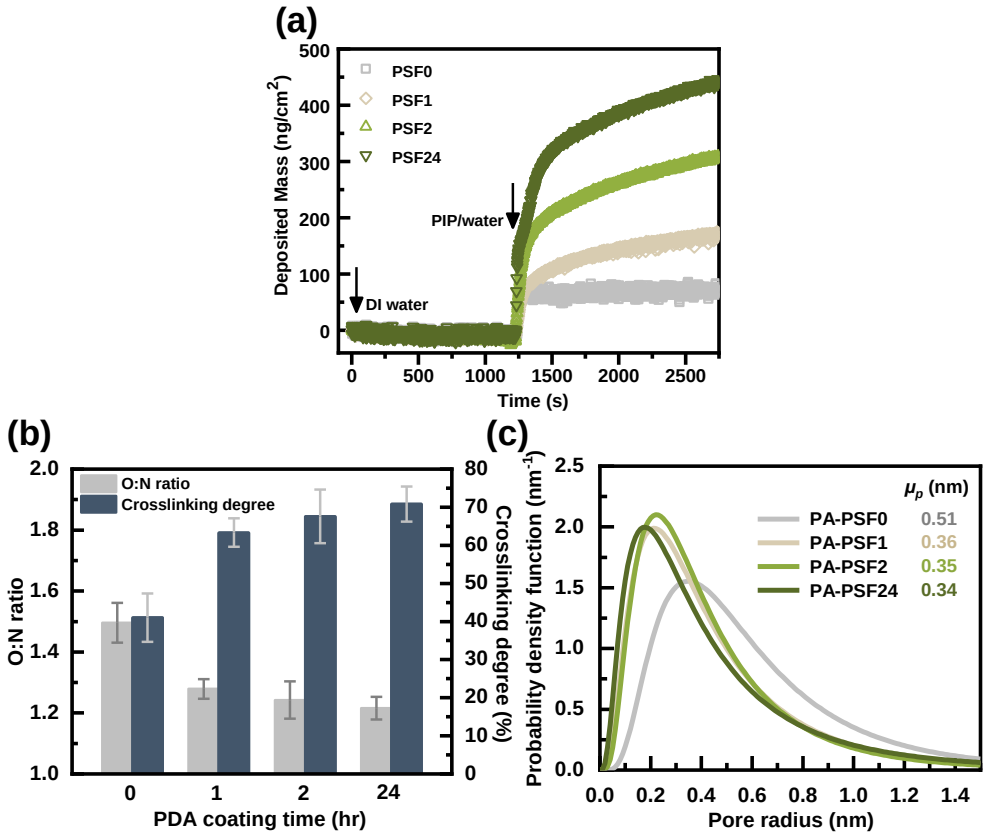

Figure 4. Membrane characterization by QCM-D, XPS and pore size analysis. (a) QCM-D measurements of PIP sorption (0.2 wt% PIP aqueous solution) onto quartz sensors coated with PSF or PDA-modified PSF following our previous study;[19] (b) oxygen/nitrogen ratio ($r_{O/N}$) based XPS results (see Supporting Information S1) and the corresponding crosslinking degree calculated by $(4\text{-}2r_{O/N})/(1+ r_{O/N})$;[34] and (c) pore size distribution and effective mean pore radius (μ_p) of PA-PSF membranes based on rejection results of glucose, raffinose, and dextran (Mw = 1k and 2k). See detailed calculations in Supporting Information S2.

Membrane separation properties.

Among the four PA-PSF membranes prepared in the current study, PA-PSF1 had the highest water permeance of 19.3 ± 0.8 $Lm^{-2}h^{-1}bar^{-1}$, showing an approximately one order of magnitude improvement over that of the control PA-PSF0 membrane (2.4 ± 0.5 $Lm^{-2}h^{-1}bar^{-1}$, Figure 5a). Further increasing in PDA coating duration decreased the membrane water permeance to 14.8 ± 0.4 $Lm^{-2}h^{-1}bar^{-1}$ for PA-PSF2 and 10.7 ± 1.5 $Lm^{-2}h^{-1}bar^{-1}$ for the PA-PSF24, possibly as a result of greater hydraulic resistance of the PDA coating. Nevertheless, the permeance values of both PA-PSF2 and PA-PSF24 were substantially greater than that of the control PA-PSF0 membrane without the PDA interlayer. This dramatic enhancement of TFNi membranes over their TFC control can be attributed to (1) the direct role of PDA interlayer as a high-permeability gutter layer to optimize the water transport pathway,[52-54] and (2) its indirect effect through the influence of the interlayer on polyamide formation (e.g., elimination of polyamide intrusion, formation of nanovoids, and increased membrane surface roughness (Figure 3)).

The PDA intercalated TFNi membranes had significantly enhanced rejection of Na_2SO_4, $MgSO_4$, $MgCl_2$, and $CaCl_2$ over that of the TFC control though the effect on NaCl was less obvious (Figure 5b). The greatly improved removal efficiency was primarily due to the formation of a more crosslinked polyamide rejection layer (Figure 4c). Nevertheless, the membrane PA-PSF24 membrane with the longest PDA

coating time had comparable salt rejection with PA-PSF2, even though the former had a higher crosslinking degree. This observation can be explained by the significantly lower water permeance of PA-PSF24, noting that the permeate solute concentration is given by the ratio of solute flux over the water flux.[3] Although the excessive PDA coating time of 24 h can cause an increase in crosslinking degree and thus reduce the solute flux through the membrane, the simultaneous decrease in water flux reduces its effectiveness in improving the permeate water quality. Our results reveal the critical importance of the coating time (and thus the thickness of the interlayer) to achieve optimized membrane separation performance.

The monovalent over divalent ion selectivity (e.g., $\alpha_{NaCl/MgSO4}$) is of great practical interest for NF applications to allow the retaining of divalent ions without the need to pay for the osmotic pressure penalty of NaCl.[19] In this study, PA-PSF2 had the highest $\alpha_{NaCl/MgSO4}$ value of 34.4 ± 1.0, far exceeding those of the control membrane PA-PSF0 and the commercial membranes NF270 and NF90. Figure 5c presents an upper bound correlation between water permeance A and $\alpha_{NaCl/MgSO4}$ for conventional TFC membranes prepared by PIP/TMC chemistry.[19] The PA-PSF1 and PA-PSF2 prepared in this study, along with a number of other TFNi membranes reported in the recent years (e.g., based on polyvinyl alcohol,[41] cellulose nanocrystals,[55] metal-organic-frameworks,[56] carbon nanotubes[6, 15] and tannic acid/Fe^{3+} complexes[19]) successfully surpass this upper bound, revealing the huge potential of such an

interlayered membrane structure.

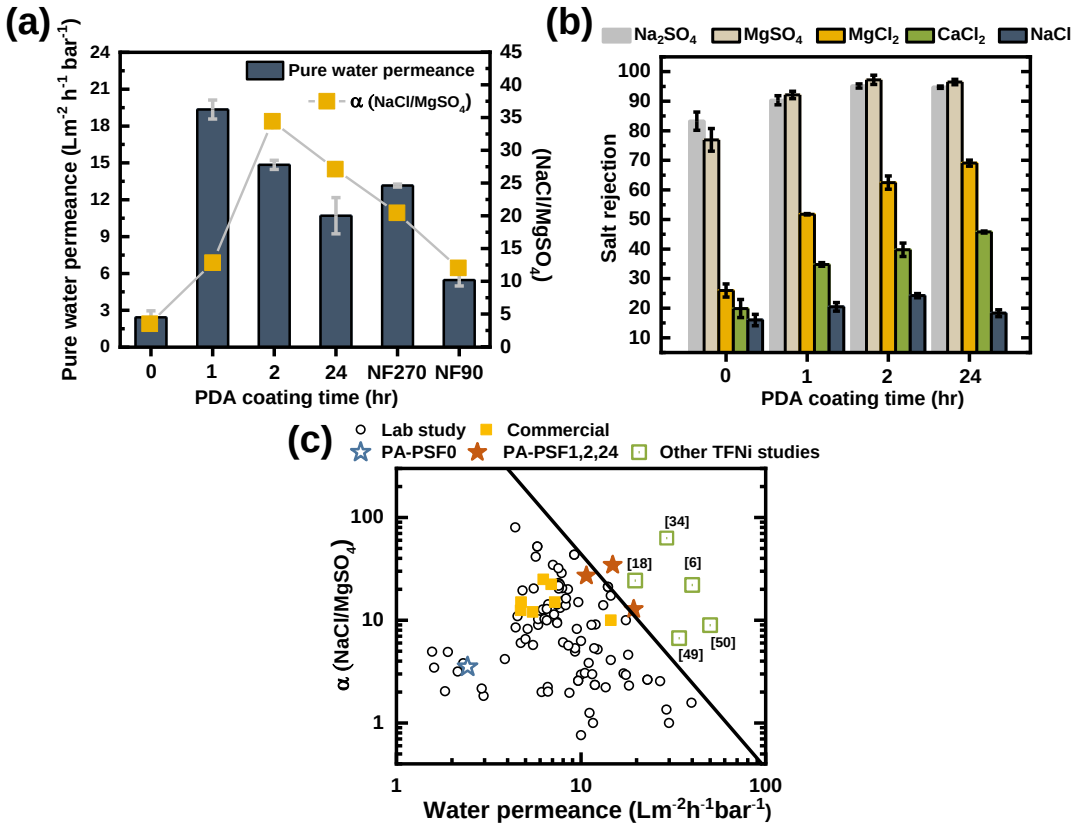

Figure 5. Membrane separation performance. (a) Pure water permeance and NaCl to $MgSO_4$ selectivity. Membranes NF270 and NF90 were included as commercially available benchmarks. (b) Salt rejection of Na_2SO_4, $MgSO_4$, $MgCl_2$, $CaCl_2$ and NaCl. Each rejection was measured using a 1000 ppm solution containing a single type of salt. The applied pressure was 50 psi and the temperature of the feed solution was approximately 24 °C. (c) Comparison the separation performance of TFNi membranes with the upper bound tradeoff for conventional TFC membranes. This trade-off between pure water permeance and NaCl/$MgSO_4$ selectivity was modified from Ref.[19] with copyright permission. The square symbols □ represent TFNi membranes published in recent literature.[6, 19, 41, 55, 56]

Mechanistic investigation of PDA interlayer.

To resolve the exact roles of the PDA interlayer on the separation properties of the resulting TFNi membranes, additional polyamide films were synthesized at a support-free interface between an aqueous PIP solution and a TMC/hexane solution

and were transferred onto PSF0 or PSF2. Therefore, the resulting membranes PAfi-PSF0 and PAfi-PSF2 had identical polyamide rejection layers but different substrates (without or with a PDA interlayer). In contrast, their counterparts PA-PSF0 and PA-PSF2 (prepared directly on substrates) not only had different support structures but also different polyamide structures (Figure 3 and Figure 4).

Figure 6a,b presents the water permeance and salt rejection of these four membranes. PA-PSF0 and PAfi-PSF0, both had identical recipes for the IP reaction and identical substrate (PSF0), show comparable water permeance of approximately 2.5 $Lm^{-2}h^{-1}bar^{-1}$. The corresponding TFNi membranes with a 2-h PDA coating (PA-PSF2 and PAfi-PSF2) both had dramatically enhanced water permeance. For example, the permeance enhancement factor of PA-PSF2 ($f_{PA\text{-}PSF2}$ = permeance of PA-PSF2 ÷ permeance of the control PA-PSF0 – 1), was 6.13. As discussed in the section "*Membrane separation properties*", this enhancement in permeance can be attributed to the improved properties of the PDA-coated substrate (f_{sub}) and/or the improved properties of the rejection layer (f_{rej}). In comparison, the permeance enhancement factor of PAfi-PSF2 ($f_{PAfi\text{-}PSF2}$) was 4.73, which is solely attributed to the enhanced substrate (f_{sub}) for which the PDA layer serves as a high permeability gutter layer. Although the concept of gutter layer is less discussed in the context of water filtration membranes, this concept has been well established for gas separation membranes to achieve enhanced permeance.[52-54, 57] A recent modeling paper[27] shows that the

411 inclusion of a high-permeability gutter layer allows gas molecules to take a much
412 shorter transport path in the rejection layer, which would also be applicable to TFNi
413 membranes (Figure 6c). In the current study, the difference between $f_{PA\text{-}PSF2}$ and
414 $f_{PAfi\text{-}PSF2}$ can be attributed to the indirect effect of the substrate on the formation of
415 polyamide rejection layer (f_{rej} = 1.40). According to recent studies, the substrate
416 serves the important roles as a reservoir for amine monomers[19, 28] and for providing
417 confinements to the interfacially degassed nanobubbles.[28, 48] In this respect, the
418 interlayer can (1) simultaneously enhance the amine monomer uptake (Figure 4a) and
419 the confinement effect (due to reduced substrate pore size[17]) to result in a rougher and
420 nanovoid-containing polyamide rejection layer (Figure 3d) and (2) also eliminate its
421 intrusion into the substrate (Figure 3c and Ref.[19]), both leading to improved water
422 transport. Nevertheless, the current study reveals that this indirect effect on rejection
423 layer (f_{rej} = 1.40) was much weaker compared to the direct "gutter layer" effect of the
424 substrate (f_{sub} = 4.73), possibly due to the weaker ability of the PIP/TMC chemistry
425 for interfacial degassing.[46]
426
427 Figure 6b shows the membrane salt rejection. PA-PSF2, PAfi-PSF0, and PAfi-PSF2
428 had comparable Na_2SO_4 and NaCl rejection values, which were significantly better
429 than the respective values of PA-PSF0. The poorer rejection performance of PA-PSF0
430 is consistent with its lower crosslinking degree (Figure 6c), possibly caused by the
431 limited availability of PIP in the PSF0 substrate.[28] In contrast, polyamide prepared on

PDA coatings (PA-PSF2) or at free interfaces (PAfi-PSF0 and PAfi-PSF2) enjoy a greater supply of PIP (e.g., see Figure 4a for PA-PSF2). In addition, previous studies[19, 28, 58] have demonstrated the greater propensity of defect formation for polyamide rejection layers prepared over relatively large substrate pores.

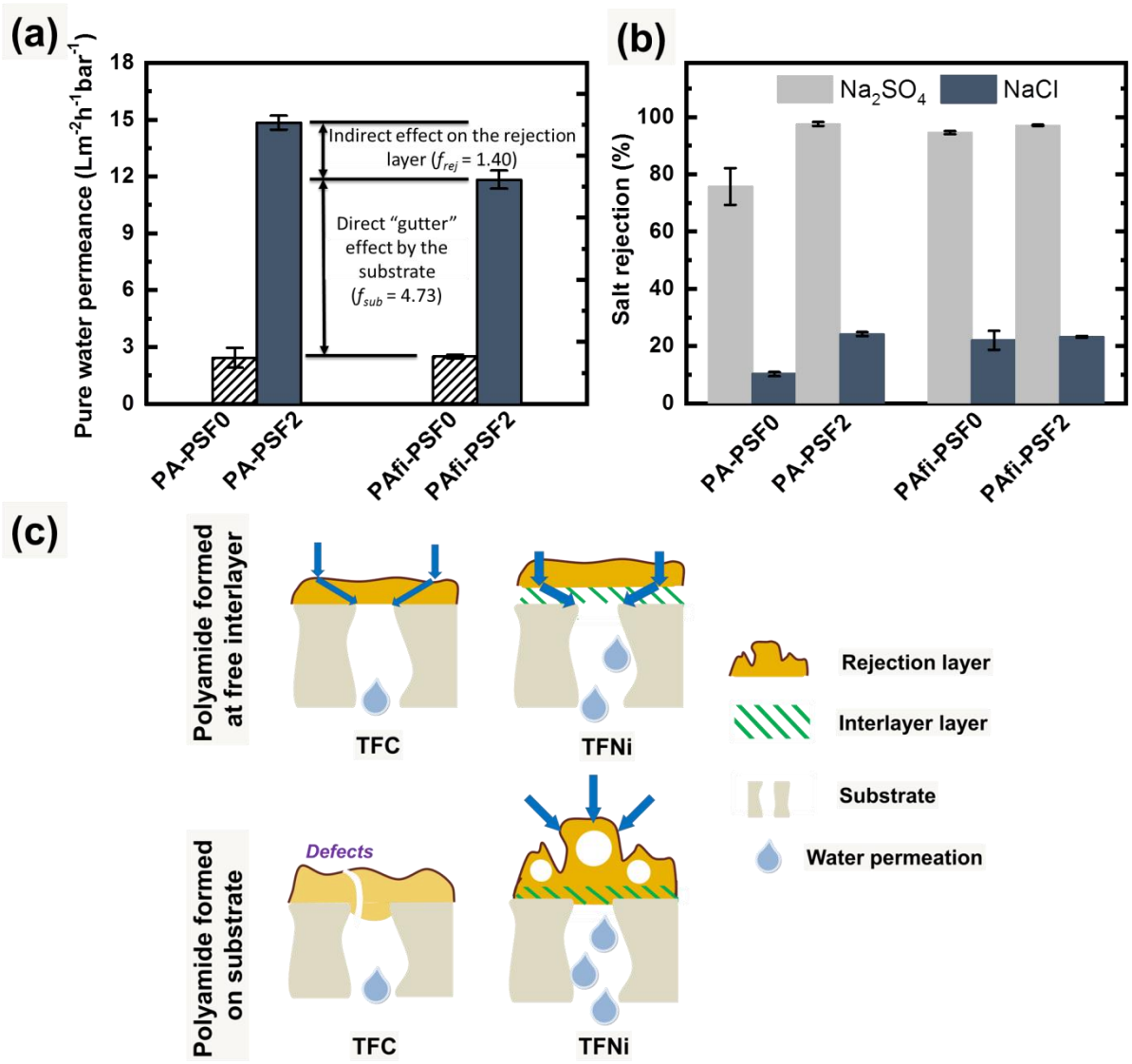

Figure 6. Mechanistic insights on the role of the interlayer. The upper panel presents (a) pure water permeance and (b) Na_2SO_4 and NaCl rejection of membranes prepared directly on the substrate (PA-PSF0 and PA-PSF2) and those prepared at a free interface (PAfi-PSF0 and PAfi-PSF2). Membrane performance was tested at an applied pressure of 50 psi at 24 °C. The lower panel presents a schematic illustration (c) of the mechanisms leading to improved

separation performances of the PDA intercalated TFNi membrane.

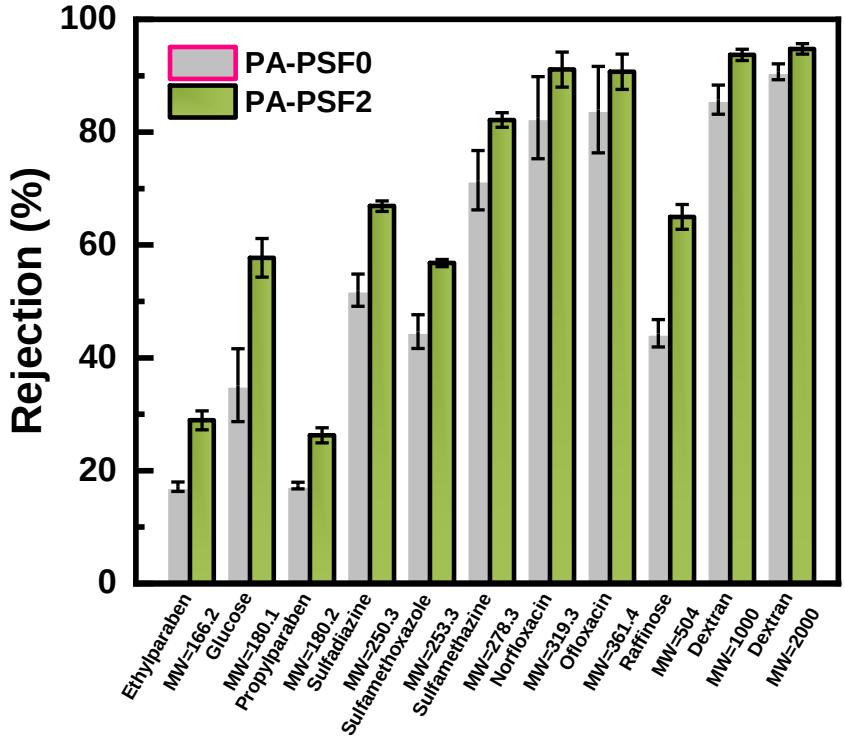

Figure 7. Membrane rejection results of the control PA-PSF0 and PA-PSF2 membrane on neutral solutes (glucose, raffinose and dextran) and TrOCs (sulfamethoxazole, sulfamethazine, norfloxacin, ofloxacin, ethylparaben and propylparaben). The rejection tests for neutral solutes (glucose, raffinose and dextran) was measured using a 200 ppm solution containing a single type of solute. For TrOCs, the rejection tests were measured using a solution containing a cocktail of six compounds (200 ppb for each TrOC). The applied pressure was 50 psi and the temperature of the feed solution was approximately 24 ℃.

IMPLICATIONS AND FUTURE PERSPECTIVES

In this study, we fabricated a PDA-intercalated TFNi NF membrane. The PDA interlayer serves as a highly permeable gutter layer for optimized water transport pathways (Figure 6c). At the same time, this interlayer prevents the intrusion of polyamide into the substrate pores, promotes the formation of nanovoids within the polyamide rejection layer, and increases its crosslinking. The direct “gutter” effect of

460 the PDA interlayer together with its indirect effects resulting from enhanced
461 polyamide layer led to an order of magnitude higher water permeance along with
462 improved solute rejection for the PDA-intercalated TFNi membrane. We further
463 reveal that the direct "gutter" effect played a more dominant role compared to the
464 indirect effects through systematic comparison of PA-PSFn membranes with their
465 counterparts synthesized at a free interface. Future studies should further investigate
466 the separate optimization of the "gutter" effect of the interlayer (with due
467 considerations to its permeability and geometry[27]) and the indirect effects (via its roles
468 as reservoir for monomers and confinement to interfacially degassed nanobubbles[28]).
469 These effects should also be further validated for the wide range of other interlayer
470 materials such as CNTs,[6, 15] polyphenols,[12, 19] and etc.[5, 56]
471
472 Existing literature on NF membrane synthesis often emphasize water permeance and
473 salt rejection. Many practical applications, however, requires high selectivity more
474 than high permeance,[59, 60] particularly for the removal of TrOCs in the context of
475 water reuse.[2, 36] The PA-PSF2 developed in this study was further tested for its
476 removal efficiency against a set of neutral hydrophilic solutes (glucose, raffinose and
477 dextran) and TrOCs (sulfamethoxazole, sulfamethazine, norfloxacin, ofloxacin,
478 ethylparaben and propylparaben). Compared to the control TFC membrane, the
479 PDA-intercalated TFNi membrane shows consistently improved removal of all
480 compounds, thanks to the increased crosslinking degree (Figure 4c) and smaller

effective membrane pore size (Figure 4d). Indeed, the multilayered structure itself offers additional opportunities for enhanced removal of TrOCs,[35, 36, 61] with the possibility to design the interlayer for widened removal spectrum and better efficiency.[62] The current study reveals the feasibility to simultaneously enhance water permeance, salt rejection, and removal of TrOCs. Future studies on systematic modelling and experimental optimization are needed to fully unleash the potential of TFNi membranes for various environmental applications.

ASSOCIATED CONTENT

The Supporting Information is available free of charge on the ACS Publications website at DOI:

S1. ATR-FTIR, magnified TEM images and XPS spectra of PA-PSF membranes; S2. Methods of determining pore size distribution; S3. Effect of pressure on membrane separation performance.

AUTHOR INFORMATION

Corresponding Author

*Phone: (+852) 2859 1976; e-mail: tangc@hku.hk

*Phone: +86 (0571) 8832 4135; e-mail: songxiaoxiao@zjut.edu.cn

Notes

The authors declare no completing financial interest.

ACKNOWLEDGEMENTS

The work is partially supported by the Joint Research Scheme between Research Grants Council of Hong Kong and National Natural Science Foundation of China (No. N_HKU706/16) as well as the Peak Discipline Construction Program in Environment and Ecology of Shanghai. We appreciate the Electron Microscopic Unit (EMU) at The University of Hong Kong for SEM and TEM sample preparation and analysis.

REFERENCES

1. Elimelech, M.; Phillip, W. A., The future of seawater desalination: energy, technology, and the environment. *Science* **2011,** *333*, (6043), 712-717.
2. Tang, C. Y.; Yang, Z.; Guo, H.; Wen, J.; Nghiem, L. D.; Cornelissen, E. R., Potable water reuse through advanced membrane technology. *Environ. Sci. Technol.* **2018,** *52*, (18), 10215-10223.
3. Yang, Z.; Guo, H.; Tang, C. Y., The upper bound of thin-film composite (TFC) polyamide membranes for desalination. *Journal of Membrane Science* **2019,** *590*, 117297.
4. Chan, W.-F.; Chen, H.-y.; Surapathi, A.; Taylor, M. G.; Shao, X.; Marand, E.; Johnson, J. K., Zwitterion functionalized carbon nanotube/polyamide nanocomposite membranes for water desalination. *ACS Nano* **2013,** *7*, (6), 5308-5319.
5. Choi, W.; Jeon, S.; Kwon, S. J.; Park, H.; Park, Y.-I.; Nam, S.-E.; Lee, P. S.; Lee, J. S.; Choi, J.; Hong, S.; Chan, E. P.; Lee, J.-H., Thin film composite reverse osmosis membranes prepared via layered interfacial polymerization. *J. Membr. Sci.* **2017,** *527*, 121-128.
6. Gao, S.; Zhu, Y.; Gong, Y.; Wang, Z.; Fang, W.; Jin, J., Ultrathin Polyamide Nanofiltration Membrane Fabricated on Brush-Painted Single-Walled Carbon Nanotube Network Support for Ion Sieving. *ACS Nano* **2019,** *13*, (5), 5278-5290.
7. Li, Y.; Su, Y.; Li, J.; Zhao, X.; Zhang, R.; Fan, X.; Zhu, J.; Ma, Y.; Liu, Y.; Jiang, Z., Preparation of thin film composite nanofiltration membrane with improved structural stability through the mediation of polydopamine. *J. Membr. Sci.* **2015,** *476*, 10-19.
8. Huang, Y.; Jin, H.; Li, H.; Yu, P.; Luo, Y., Synthesis and characterization of a polyamide thin film composite membrane based on a polydopamine coated support layer for forward osmosis. *RSC Adv.* **2015,** *5*, (128), 106113-106121.
9. Ingole, P. G.; Choi, W.; Kim, K. H.; Park, C. H.; Choi, W. K.; Lee, H. K., Synthesis, characterization and surface modification of PES hollow fiber membrane support with polydopamine and thin film composite for energy generation. *Chem. Eng. J.* **2014,** *243*, 137-146.
10. Han, G.; Zhang, S.; Li, X.; Widjojo, N.; Chung, T.-S., Thin film composite forward osmosis membranes based on polydopamine modified polysulfone substrates with enhancements in both water flux and salt rejection. *Chem. Eng. Sci.* **2012,** *80*, 219-231.
11. Wu, X.; Li, Y.; Cui, X.; Wang, J.; Cao, X.; Zhang, P.; Zheng, L., Adsorption-Assisted Interfacial Polymerization toward Ultrathin Active Layers for Ultrafast Organic Permeation. *ACS Appl. Mater. Interfaces* **2018,** *10*, (12), 10445-10453.
12. Zhang, X.; Lv, Y.; Yang, H.-C.; Du, Y.; Xu, Z.-K., Polyphenol Coating as an Interlayer for Thin-Film Composite Membranes with Enhanced Nanofiltration Performance. *ACS Appl. Mater. Interfaces* **2016,** *8*, (47), 32512-32519.

13. Zhu, Y.; Dou, P.; He, H.; Lan, H.; Xu, S.; Zhang, Y.; He, T.; Niu, J., Improvement of permeability and rejection of an acid resistant polysulfonamide thin-film composite nanofiltration membrane by a sulfonated poly(ether ether ketone) interlayer. *Sep. Purif. Technol.* **2020,** *239*, 116528.
14. Shah, A. A.; Cho, Y. H.; Choi, H.-g.; Nam, S.-E.; Kim, J. F.; Kim, Y.; Park, Y.-I.; Park, H., Facile integration of halloysite nanotubes with bioadhesive as highly permeable interlayer in forward osmosis membranes. *J. Ind. Eng. Chem.* **2019,** *73*, 276-285.
15. Zhou, Z.; Hu, Y.; Boo, C.; Liu, Z.; Li, J.; Deng, L.; An, X., High-Performance Thin-Film Composite Membrane with an Ultrathin Spray-Coated Carbon Nanotube Interlayer. *Environ. Sci. Technol. Lett.* **2018,** *5*, (5), 243-248.
16. Wu, M.-B.; Lv, Y.; Yang, H.-C.; Liu, L.-F.; Zhang, X.; Xu, Z.-K., Thin film composite membranes combining carbon nanotube intermediate layer and microfiltration support for high nanofiltration performances. *J. Membr. Sci.* **2016,** *515*, 238-244.
17. Zhang, M.; Jin, W.; Yang, F.; Duke, M. C.; Dong, Y.; Tang, C. Y., Engineering Nano-Composite Interlayer for Novel Ceramic-based Forward Osmosis Membrane with Enhanced Performance. *Environ. Sci. Technol.* **2020,** *54*, (12), 7715-7724.
18. Yang, X.; Du, Y.; Zhang, X.; He, A.; Xu, Z.-K., Nanofiltration Membrane with a Mussel-Inspired Interlayer for Improved Permeation Performance. *Langmuir* **2017,** *33*, (9), 2318-2324.
19. Yang, Z.; Zhou, Z. W.; Guo, H.; Yao, Z.; Ma, X. H.; Song, X.; Feng, S. P.; Tang, C. Y., Tannic Acid/Fe(3+) Nanoscaffold for Interfacial Polymerization: Toward Enhanced Nanofiltration Performance. *Environ. Sci. Technol.* **2018,** *52*, (16), 9341-9349.
20. Zhao, W.; Liu, H.; Liu, Y.; Jian, M.; Gao, L.; Wang, H.; Zhang, X., Thin-Film Nanocomposite Forward-Osmosis Membranes on Hydrophilic Microfiltration Support with an Intermediate Layer of Graphene Oxide and Multiwall Carbon Nanotube. *ACS Appl. Mater. Interfaces* **2018,** *10*, (40), 34464-34474.
21. Yang, H.-C.; Luo, J.; Lv, Y.; Shen, P.; Xu, Z.-K., Surface engineering of polymer membranes via mussel-inspired chemistry. *J. Membr. Sci.* **2015,** *483*, 42-59.
22. Lee, H.; Dellatore, S. M.; Miller, W. M.; Messersmith, P. B., Mussel-inspired surface chemistry for multifunctional coatings. *Science* **2007,** *318*, (5849), 426-430.
23. Choi, H.-g.; Shah, A. A.; Nam, S.-E.; Park, Y.-I.; Park, H., Thin-film composite membranes comprising ultrathin hydrophilic polydopamine interlayer with graphene oxide for forward osmosis. *Desalination* **2019,** *449*, 41-49.
24. Yang, Z.; Huang, X.; Wang, J.; Tang, C.; Engineering, Novel polyethyleneimine/TMC-based nanofiltration membrane prepared on a polydopamine coated substrate. *Frontiers Chemi. Sci. Eng.* **2018,** *12*, (2), 273-282.
25. Zhu, J.; Hou, J.; Zhang, R.; Yuan, S.; Li, J.; Tian, M.; Wang, P.; Zhang, Y.; Volodin, A.; Van der Bruggen, B., Rapid water transport through controllable, ultrathin polyamide nanofilms for high-performance nanofiltration. *J. Mater. Chem. A*

2018, *6*, (32), 15701-15709.
26. Khanzada, N. K.; Farid, M. U.; Kharraz, J. A.; Choi, J.; Tang, C. Y.; Nghiem, L. D.; Jang, A.; An, A. K., Removal of organic micropollutants using advanced membrane-based water and wastewater treatment: A review. *Journal of Membrane Science* **2020,** *598*, 117672.
27. Kattula, M.; Ponnuru, K.; Zhu, L.; Jia, W.; Lin, H.; Furlani, E. P., Designing ultrathin film composite membranes: the impact of a gutter layer. *Sci. Rep.* **2015,** *5*, (1), 15016.
28. Peng, L. E.; Yao, Z.; Yang, Z.; Guo, H.; Tang, C. Y., Dissecting the Role of Substrate on the Morphology and Separation Properties of Thin Film Composite Polyamide Membranes: Seeing Is Believing. *Environmental Science & Technology* **2020,** *54*, (11), 6978-6986.
29. Jiang, Z.; Karan, S.; Livingston, A. G., Water transport through ultrathin polyamide nanofilms used for reverse osmosis. *Adv. Mater.* **2018,** *30*, (15), 1705973.
30. Pacheco, F.; Sougrat, R.; Reinhard, M.; Leckie, J. O.; Pinnau, I., 3D visualization of the internal nanostructure of polyamide thin films in RO membranes. *J. Membr. Sci.* **2016,** *501*, 33-44.
31. Yang, Z.; Wu, Y.; Wang, J.; Cao, B.; Tang, C. Y., In situ reduction of silver by polydopamine: A novel antimicrobial modification of a thin-film composite polyamide membrane. *Environ. Sci. Technol.* **2016,** *50*, (17), 9543-50.
32. Yang, Z.; Wu, Y.; Guo, H.; Ma, X.-H.; Lin, C.-E.; Zhou, Y.; Cao, B.; Zhu, B.-K.; Shih, K.; Tang, C. Y., A novel thin-film nano-templated composite membrane with in situ silver nanoparticles loading: Separation performance enhancement and implications. *J. Membr. Sci.* **2017,** *544*, 351-358.
33. Yang, Z.; Huang, X.; Ma, X.-h.; Zhou, Z.-w.; Guo, H.; Yao, Z.; Feng, S.-P.; Tang, C. Y., Fabrication of a novel and green thin-film composite membrane containing nanovoids for water purification. *J. Membr. Sci.* **2019,** *570-571*, 314-321.
34. Yang, Z.; Guo, H.; Yao, Z.-k.; Mei, Y.; Tang, C. Y., Hydrophilic silver nanoparticles induce selective nanochannels in thin film nanocomposite polyamide membranes. *Environmental Science & Technology* **2019,** *53*, (9), 5301-5308.
35. Guo, H.; Yao, Z.; Yang, Z.; Ma, X.; Wang, J.; Tang, C. Y., A one-step rapid assembly of thin film coating using green coordination complexes for enhanced removal of trace organic contaminants by membranes. *Environ. Sci. Technol.* **2017,** *51*, (21), 12638-12643.
36. Guo, H.; Deng, Y.; Tao, Z.; Yao, Z.; Wang, J.; Lin, C.; Zhang, T.; Zhu, B.; Tang, C. Y., Does Hydrophilic Polydopamine Coating Enhance Membrane Rejection of Hydrophobic Endocrine-Disrupting Compounds? *Environ. Sci. & Technol. Lett.* **2016,** *3*, (9), 332-338.
37. Fujioka, T.; Kodamatani, H.; Takeuchi, H.; Tanaka, H.; Nghiem, L. D., Online monitoring of N-nitrosodimethylamine for the removal assurance of 1,4-dioxane and other trace organic compounds by reverse osmosis. *Environ. Sci. Water Res. Technol.* **2018,** *4*, (12), 2021-2028.

636 38. Jin, X.; Shan, J.; Wang, C.; Wei, J.; Tang, C. Y., Rejection of pharmaceuticals by
637 forward osmosis membranes. *J. Hazard. Mater.* **2012,** *227-228*, 55-61.
638 39. Arena, J. T.; McCloskey, B.; Freeman, B. D.; McCutcheon, J. R., Surface
639 modification of thin film composite membrane support layers with polydopamine:
640 enabling use of reverse osmosis membranes in pressure retarded osmosis. *J. Membr.*
641 *Sci.* **2011,** *375*, (1), 55-62.
642 40. Yang, H.-C.; Liao, K.-J.; Huang, H.; Wu, Q.-Y.; Wan, L.-S.; Xu, Z.-K.,
643 Mussel-inspired modification of a polymer membrane for ultra-high water
644 permeability and oil-in-water emulsion separation. *J. Mater. Chem. A* **2014,** *2*, (26),
645 10225-10230.
646 41. Tan, Z.; Chen, S.; Peng, X.; Zhang, L.; Gao, C., Polyamide membranes with
647 nanoscale turing structures for water purification. *Science* **2018,** *360*, (6388), 518-521.
648 42. Tang, C. Y.; Kwon, Y.-N.; Leckie, J. O., Effect of membrane chemistry and
649 coating layer on physiochemical properties of thin film composite polyamide RO and
650 NF membranes: I. FTIR and XPS characterization of polyamide and coating layer
651 chemistry. *Desalination* **2009,** *242*, (1-3), 149-167.
652 43. Gong, G.; Wang, P.; Zhou, Z.; Hu, Y., New insights into the role of an interlayer
653 for the fabrication of highly selective and permeable thin-film composite
654 nanofiltration membrane. *ACS Appl. Mater. Interfaces* **2019,** *11*, (7), 7349-7356.
655 44. Lin, L.; Lopez, R.; Ramon, G. Z.; Coronell, O., Investigating the void structure of
656 the polyamide active layers of thin-film composite membranes. *J. Membr. Sci.* **2016,**
657 *497*, 365-376.
658 45. Pacheco, F. A.; Pinnau, I.; Reinhard, M.; Leckie, J. O., Characterization of
659 isolated polyamide thin films of RO and NF membranes using novel TEM techniques.
660 *J. Membr. Sci.* **2010,** *358*, (1-2), 51-59.
661 46. Ma, X.-H.; Yao, Z.; Yang, Z.; Guo, H.; Xu, Z.; Tang, C. Y.; Elimelech, M.,
662 Nanofoaming of Polyamide Desalination Membranes to Tune Permeability and
663 Selectivity. *Environ. Sci. Technol. Lett.* **2018,** *5*, (2), 123-130.
664 47. Peng, L. E.; Yao, Z.; Liu, X.; Deng, B.; Guo, H.; Tang, C. Y., Tailoring Polyamide
665 Rejection Layer with Aqueous Carbonate Chemistry for Enhanced Membrane
666 Separation: Mechanistic Insights, Chemistry-Structure-Property Relationship, and
667 Environmental Implications. *Environ. Sci. Technol.* **2019,** *53*, (16), 9764-9770.
668 48. Song, X.; Gan, B.; Yang, Z.; Tang, C. Y.; Gao, C., Confined nanobubbles shape
669 the surface roughness structures of thin film composite polyamide desalination
670 membranes. *Journal of Membrane Science* **2019,** *582*, 342-349.
671 49. Ukrainsky, B.; Ramon, G. Z., Temperature measurement of the reaction zone
672 during polyamide film formation by interfacial polymerization. *J. Membr. Sci.* **2018,**
673 *566*, 329-335.
674 50. Song, X.; Gan, B.; Qi, S.; Guo, H.; Tang, C. Y.; Zhou, Y.; Gao, C., Intrinsic
675 nanoscale structure of thin film composite polyamide membranes: Connectivity,
676 defects, and structure-property correlation. *Environmental Science & Technology*
677 **2020,** *54*, (6), 3559-3569.

678 51. Ma, X.; Yang, Z.; Yao, Z.; Guo, H.; Xu, Z.; Tang, C. Y., Tuning roughness
679 features of thin film composite polyamide membranes for simultaneously enhanced
680 permeability, selectivity and anti-fouling performance. *Journal of Colloid and*
681 *Interface Science* **2019,** *540*, 382-388.
682 52. Kouketsu, T.; Duan, S.; Kai, T.; Kazama, S.; Yamada, K., PAMAM dendrimer
683 composite membrane for CO2 separation: Formation of a chitosan gutter layer. *J.*
684 *Membr. Sci.* **2007,** *287*, (1), 51-59.
685 53. Li, T.; Pan, Y.; Peinemann, K. V.; Lai, Z., Carbon dioxide selective mixed matrix
686 composite membrane containing ZIF-7 nano-fillers. *J. Membr. Sci.* **2013,** *425-426*,
687 235-242.
688 54. Liang, C. Z.; Liu, J. T.; Lai, J. Y.; Chung, T. S., High-performance multiple-layer
689 PIM composite hollow fiber membranes for gas separation. *J. Membr. Sci.* **2018,** *563*,
690 93-106.
691 55. Wang, J.-J.; Yang, H.-C.; Wu, M.-B.; Zhang, X.; Xu, Z.-K., Nanofiltration
692 membranes with cellulose nanocrystals as an interlayer for unprecedented
693 performance. *J. Mater. Chem. A* **2017,** *5*, (31), 16289-16295.
694 56. Wang, Z.; Wang, Z.; Lin, S.; Jin, H.; Gao, S.; Zhu, Y.; Jin, J.,
695 Nanoparticle-templated nanofiltration membranes for ultrahigh performance
696 desalination. *Nat. Commun.* **2018,** *9*, (1), 2004.
697 57. Chen, H. Z.; Thong, Z.; Li, P.; Chung, T. S., High performance composite hollow
698 fiber membranes for CO2/H2 and CO2/N2 separation. *Int. J. Hydrog. Energy* **2014,**
699 *39*, (10), 5043-5053.
700 58. Huang, L.; McCutcheon, J. R., Impact of support layer pore size on performance
701 of thin film composite membranes for forward osmosis. *J. Membr. Sci.* **2015,** *483*,
702 25-33.
703 59. Werber, J. R.; Deshmukh, A.; Elimelech, M., The critical need for increased
704 selectivity, not increased water permeability, for desalination membranes. *Environ. Sci.*
705 *Technol. Lett.* **2016,** *3*, (4), 112-120.
706 60. Patel, S. K.; Ritt, C.; Deshmukh, A.; Wang, Z.; Qin, M.; Epsztein, R.; Elimelech,
707 M., The relative insignificance of advanced materials in enhancing the energy
708 efficiency of desalination technologies. *Energy Environ. Sci.* **2020,** *13*, (1694-1710).
709 61. Guo, H.; Deng, Y.; Yao, Z.; Yang, Z.; Wang, J.; Lin, C.; Zhang, T.; Zhu, B.; Tang,
710 C. Y., A highly selective surface coating for enhanced membrane rejection of
711 endocrine disrupting compounds: Mechanistic insights and implications. *Water Res.*
712 **2017,** *121*, 197-203.
713 62. Guo, H.; Peng, L. E.; Yao, Z.; Yang, Z.; Ma, X.; Tang, C. Y., Non-Polyamide
714 Based Nanofiltration Membranes Using Green Metal–Organic Coordination
715 Complexes: Implications for the Removal of Trace Organic Contaminants. *Environ.*
716 *Sci. Technol.* **2019,** *53*, (5), 2688-2694.
717